

PATIENT-AWARE MULTIMODAL RGB-HSI FUSION VIA INCREMENTAL HEURISTIC META-LEARNING FOR ORAL LESION CLASSIFICATION

Rupam Mukherjee^{†1} Rajkumar Daniel^{†1} Soujanya Hazra^{†2} Shirin Dasgupta³ Subhamoy Mandal¹

¹ School of Medical Science & Technology, IIT Kharagpur, India

² Department of Electrical Engineering, IIT Kharagpur, India

³ Dr. B.C. Roy Multispeciality Medical Research Centre, IIT Kharagpur, India

ABSTRACT

Early detection of oral cancer and potentially malignant diseases is a major challenge in low-resource settings due to the scarcity of annotated data. We provide a unified approach for four-class oral lesion classification that incorporates deep learning, spectral analysis, and demographic data. A pathologist-verified subset of oral cavity images was curated from a publicly available dataset. Oral cavity pictures were processed using a fine-tuned ConvNeXt-v2 network for deep embeddings before being translated into the hyperspectral domain using a reconstruction algorithm. Haemoglobin-sensitive, textural, and spectral descriptors were obtained from the reconstructed hyperspectral cubes and combined with demographic data. Multiple machine-learning models were evaluated using patient-specific validation. Finally, an incremental heuristic meta-learner (IHML) was developed that merged calibrated base classifiers via probabilistic feature stacking and uncertainty-aware abstraction of multimodal representations with patient-level smoothing. By decoupling evidence extraction from decision fusion, IHML stabilizes predictions in heterogeneous, small-sample medical datasets. On an unseen test set, our proposed model achieved a macro F1 of 66.23% and an overall accuracy of 64.56%. The findings demonstrate that RGB-to-hyperspectral reconstruction and ensemble meta-learning improve diagnostic robustness in real-world oral lesion screening.

Index Terms— Multi-modal learning, oral lesion classification, heuristics, hyperspectral features, meta-classifier.

1. INTRODUCTION AND RELATED WORKS

Oral cancer (OCA) and oral potentially malignant disorders (OPMD) are still significant causes of morbidity and mortality, particularly in South and Southeast Asia. Early detection is crucial, but clinical screening is often hindered by subjectivity and a shortage of professionals [1]. Artificial intelligence and computer vision, particularly deep convolutional models and transfer learning, have shown strong potential for improving lesion detection and risk assessment.

Existing datasets, limited by small sample sizes, inconsistent collection methods, and poor clinical metadata, continue to affect the reliability and practical translation of AI-based oral screening systems. The recent study [2] aims to close this gap by enabling image-based classification enriched with contextual factors, such as age, gender, and behavioral risks. However, most existing methods rely solely on RGB images, overlooking spectral and textural information that could enhance lesion classification. Advances in image restoration networks have enhanced the recovery of fine structural details in impaired medical and photographic data. The multi-stage progressive restoration model MPRNet [3] enhances texture, contrast, and lighting uniformity, improving visual quality while preserving diagnostically relevant cues for feature extraction. In parallel, ConvNeXt-v2 [4] offers high-quality embeddings with modern convolution efficiency. On the classification side, ensemble learning and meta-modeling techniques have demonstrated strong generalization in heterogeneous biomedical data [5]. Gradient-boosting and tree-based models effectively capture nonlinear dependencies, but combining multiple calibrated learners can further stabilize predictions and handle multimodal feature spaces. However, existing multimodal oral lesion studies typically rely on either single-stage feature concatenation or end-to-end classifiers, which are sensitive to feature redundancy, dataset imbalance, and intra-patient variability. In contrast, our approach explicitly models predictive uncertainty and enforces patient-level consistency, both of which are critical for real-world screening scenarios with heterogeneous image quality.

To the best of our knowledge, this is among the first studies to integrate spectrally enriched representations, hand-crafted biomarkers, and clinical priors within an uncertainty-aware meta-learning framework for oral lesion classification. Our key contributions are as follows: (1) We present a multimodal ensemble process for four-class oral lesion classification using RGB deep embeddings, hyperspectral reconstruction, customized spectral-textural descriptors, and demographic metadata. (2) To ensure diagnostic reliability, we curate a pathologist-verified subset of the dataset, process each image with a fine-tuned encoder, and rebuild 31-band

[†]These authors contributed equally.

hyperspectral cubes to generate physiologically significant features. (3) For reliable and uncertainty-aware predictions, we build an IHML that combines calibrated classifier probabilities via probabilistic stacking and patient-level posterior smoothing. (4) We demonstrate high and consistent performance on a patient-wise unseen test split, demonstrating that deep morphological cues, spectral indices, and clinical priors increase real-world oral lesion screening diagnostic robustness.

This paper is summarized as follows. Section 2 describes the dataset. Section 3 defines our approach. Section 4 summarizes the experimental findings. We conclude our work in Section 5.

2. DATASET

We used an openly available oral lesion dataset [2]. The entire dataset comprises 3,000 white-light oral cavity photos collected from 714 patients and categorized into four groups: healthy, benign, OPMD, and OCA. Each image contains polygonal boundaries of the mouth cavity or lesion locations, along with patient-specific metadata such as age, gender, smoking history, alcohol consumption, and betel chewing. In this investigation, each image was manually evaluated by an in-house expert oral pathologist. Images that lacked diagnostic reliability were excluded. Defocus, motion blur, poor illumination, overexposure, strong shadows, and images that did not depict the underlying lesion were among the most common difficulties. This clinical filtering ensured that only photos suitable for downstream processing were retained. Each image was cropped to the region of interest containing the lesion and resized to 512×512 pixels to ensure uniform spatial resolution across modalities. After curation, the final collection included 2438 pictures from 653 patients. Class labels were retained from the original dataset.

The curated cohort exhibits a naturally imbalanced class distribution, reflecting real-world oral screening settings. OPMD is the largest category (46.5% of photos), followed by benign lesions (24.9%), healthy samples (24.3%), and OCA (4.3%). The majority of patients are between 31 and 70 years old, and males are more prevalent across all age groups, consistent with epidemiological trends in oral lesions. Despite this imbalance, all models were trained and evaluated using stratified subject-wise splits to prevent information leakage, as each subject contributed multiple images acquired under varying viewpoints and illumination conditions, which encouraged aggregation and posterior smoothing during inference.

3. METHODOLOGY

The proposed pipeline combines deep morphological embeddings, handcrafted spectral features, and patient-level clinical data into a unified multimodal representation for oral lesion

classification. The proposed framework is illustrated in Fig. 2 and consists of five major stages: (1) generating HSI from RGB images, (2) deep representation extraction, (3) feature set for lesion separation, (3) multimodal feature fusion, and (5) incremental heuristic meta-learner (IHML).

3.1. Generating Hyperspectral Images from RGB Images

Hyperspectral photos capture reflectance across tens to hundreds of small spectral bands, usually across the visible spectrum, unlike RGB images, which use only three broad channels for red, green, and blue wavelengths. True hyperspectral oral images require expensive, complex equipment, making them unsuitable for large-scale or low-resource screening. Research on producing hyperspectral images from RGB images began in the early 2000s [6], and in recent years, CNNs and other machine learning approaches have been widely applied [7, 8].

In this work, we fine-tuned the Multi-Stage Progressive Image Restoration Network (MPRNet) [3] to recover hyperspectral representations from RGB oral lesion images. The network creates a hyperspectral cube $H \in \mathbb{R}^{512 \times 512 \times 31}$ from an RGB region of interest $I \in \mathbb{R}^{512 \times 512 \times 3}$, sampling spectral bands at 10-nm intervals from 400-700 nm. The RGB image is extended along the spectral dimension using the reconstructed cube, preserving the image-plane spatial structure. Figure 1 depicts the conceptual difference between RGB and hyperspectral representations. The spatial dimensions (x, y) correspond to the image plane, but the spectral dimension (z) stores wavelength-dependent reflectance differences across many channels, which are then used for feature extraction. In particular, MPRNet [3] uses the peak signal-to-noise ratio (PSNR) as an index to evaluate the accuracy of the generated hyperspectral image. A PSNR of 33.50 dB indicates consistent reconstruction quality suitable for downstream feature extraction. The reconstructed hyperspectral representations are not intended to replace physically acquired HSI, but to provide spectrally enriched cues that enable wavelength-localized feature extraction from RGB data in resource-constrained settings.

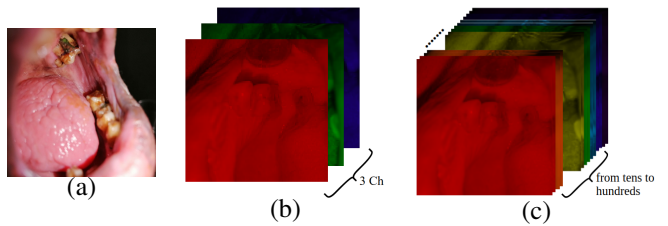


Fig. 1. Examples of RGB and hyperspectral images. (a) displays the subject. (b) depicts the channel configuration with a general camera, while (c) shows the channel structure with a hyperspectral camera.

3.2. Deep Representation Extraction

Following hyperspectral reconstruction, we extract various deep and handcrafted representations to capture global morphological patterns of oral lesions and fine-grained spectral-textural features. Deep morphological features are recovered from the RGB region of interest (ROI) using ConvNeXt-v2 [4]. The network is initialized with ImageNet-pretrained weights and fine-tuned on the curated oral lesion dataset to match domain-specific visual patterns. After training, the classification head is removed, and the final global average pooling layer output is employed as a compact deep embedding. This computationally efficient approach encodes high-level structural information, color gradients, and contextual lesion morphology. Each ROI’s reconstructed hyperspectral cube is kept for downstream feature computation.

3.3. Feature Set for Lesion Separation

We extracted three complementary families of features that provide a compact yet physiologically grounded representation for the lesion:

1. Haemoglobin-Sensitive Spectral Biomarkers: Oxy- and deoxy-haemoglobin exhibit characteristic absorption behaviour around 545–575 nm. We extract multiple ratio-metric features that emphasize relative attenuation in these bands. These include the well-established reflectance ratio R_{545}/R_{575} , the normalized difference index $NDI = (R_{545} - R_{575})/(R_{545} + R_{575})$ [9], a pseudo-Hb contrast using $(R_{560} - R_{600})$, and short-range spectral scatter slopes estimated by local linear fits across narrow spectral windows.

2. Multiscale Texture and Structural Descriptors: We extracted texture features that capture the spatial patterns present in oral lesions. Grey-level co-occurrence matrix (GLCM) statistics describe second-order textures such as contrast and homogeneity. Local Binary Patterns (LBP) capture fine surface details and local intensity changes. Gabor filters measure texture at multiple scales and orientations. SIFT descriptors detect [10] and summarize key local structures within the lesion regions.

3. Spectral-Shape and Unmixing-Oriented Features: We also extract features that describe the overall shape of the reflectance spectrum. These include band-wise maxima and minima, the wavelengths at which they occur, peak-to-valley differences, and simple slope and curvature measures. Such features reflect changes in chromophore composition, including keratin, melanin, and oxygenated blood [11]. These descriptors complement haemoglobin-sensitive ratios by capturing global spectral trends that are less sensitive to absolute reflectance magnitude and illumination variability.

Together, these feature families provide complementary views of lesion morphology, local tissue structure, and spectral behavior, enabling robust discrimination across visually overlapping diagnostic categories.

3.4. Multimodal Feature Fusion

Deep ConvNeXt-v2 embeddings and handcrafted feature sets capture complementary aspects of lesion appearance. The deep representation encodes global morphology, color gradients, and high-level contextual structure, while the handmade descriptors give fine-grained spectral variations, local texture patterns, and clinically relevant demographic risk factors. To construct a unified representation, all feature modalities were concatenated into a single multimodal vector:

$$\mathbf{x} = \mathbf{z}_{\text{deep}} \parallel \mathbf{z}_{\text{hae}} \parallel \mathbf{z}_{\text{tex}} \parallel \mathbf{z}_{\text{spec}} \parallel \mathbf{z}_{\text{demo}},$$

where $\mathbf{z}_{\text{deep}} \in \mathbb{R}^{768}$, $\mathbf{z}_{\text{hae}} \in \mathbb{R}^{46}$, $\mathbf{z}_{\text{tex}} \in \mathbb{R}^{58}$, $\mathbf{z}_{\text{spec}} \in \mathbb{R}^{31}$, and $\mathbf{z}_{\text{demo}} \in \mathbb{R}^5$ represents the ConvNeXt-v2, haemoglobin-sensitive, texture, spectral-style, and demographic features, respectively. Potential feature collinearity is mitigated through architectural design rather than linear compression. Specifically, features are normalized independently within each modality to avoid scale-induced dominance, and the subsequent IHML uses calibrated probabilistic outputs rather than raw feature activations. Tree-based base learners use hierarchical splits to suppress redundant dimensions, whereas the meta-learning stage aggregates uncertainty-aware posterior statistics, compressing correlated evidence into low-variance confidence measures.

3.5. Incremental Heuristic Meta-Learner

The IHML is the foundation of our framework. It incorporates the decisions from multiple heterogeneous classifiers, extracts uncertainty-aware meta-features, and uses iterative posterior smoothing to ensure patient-level prediction consistency. This architecture enables robust multiclass classification despite varying image quality and significant intra-patient correlation.

1. Base Learners and Probability Estimation: For each multimodal feature vector \mathbf{x} , we train four calibrated base models: LightGBM, extra trees, gradient boosting, and isotonic-calibrated logistic regression. Each model g_m generates a probability distribution for the four lesion classes: $\mathbf{p}^{(m)} = g_m(\mathbf{x}) \in [0, 1]^4$. These probability vectors constitute the first layer of the IHML stack.

2. Confidence-Aware Probabilistic Features: We use scalar confidence statistics from $\mathbf{p}^{(m)}$ to assess the reliability of each base model. These include the highest class confidence, the top-two class margin, and the Shannon entropy. We denote this transformation as $\psi(\cdot)$: $\mathbf{c}^{(m)} = \psi(\mathbf{p}^{(m)})$, where $\mathbf{c}^{(m)}$ is a low-dimensional vector encoding uncertainty and inter-class separation. The meta-feature vector is created by concatenating all base probabilities and confidence features.

$$\mathbf{h} = \Phi(\mathbf{p}^{(1)}, \dots, \mathbf{p}^{(M)}, \mathbf{c}^{(1)}, \dots, \mathbf{c}^{(M)}) \quad (1)$$

where $\Phi(\cdot)$ stacks all components into a single representation.

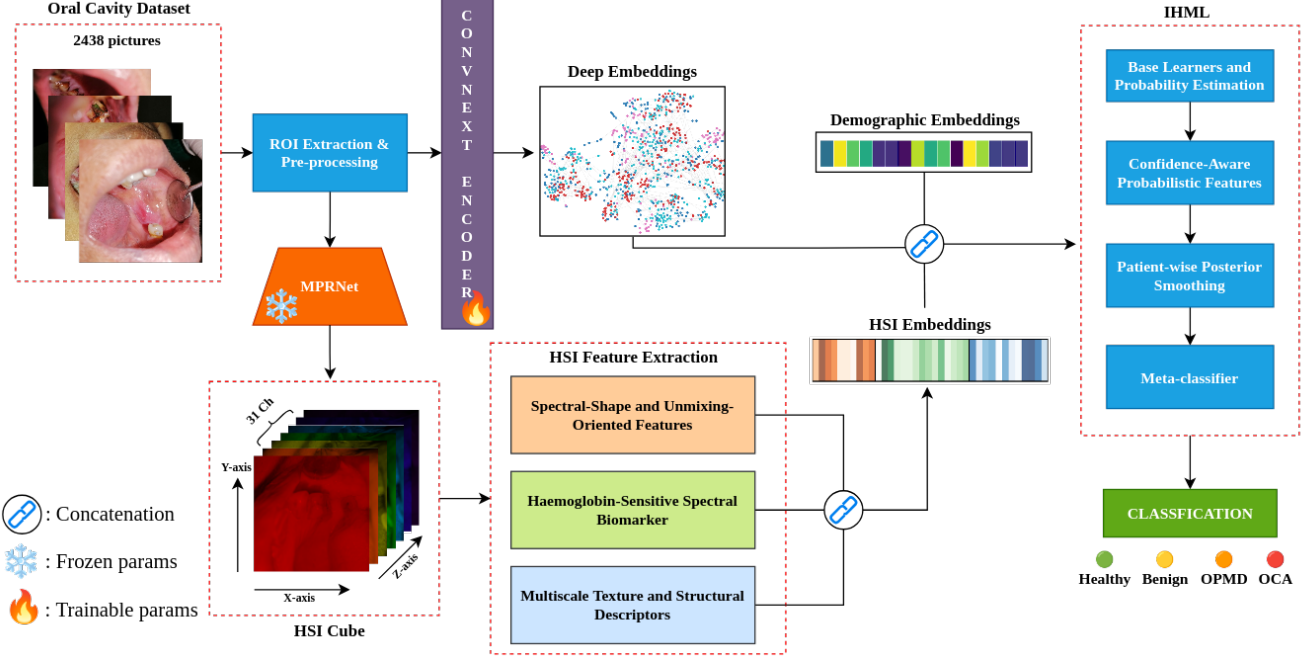


Fig. 2. Illustration of the proposed multimodal pipeline combines RGB deep embeddings, hyperspectral features, and demographic metadata to predict oral lesions at the patient level using IHML.

3. Patient-wise Posterior Smoothing: Because multiple images come from the same patient, the classifier’s outputs may exhibit unexpected intra-subject variation. IHML mitigates this effect through a patient-level refining stage. We iteratively update the probability vector for sample i in patient group $g(i)$ as follows:

$$\mathbf{p}_i^{(t+1)} = (1 - \alpha) \mathbf{p}_i^{(t)} + \alpha \bar{\mathbf{p}}_{g(i)}^{(t)}, \quad (2)$$

where $\bar{\mathbf{p}}_{g(i)}$ is the mean probability of all samples from the same patient, and α controls the influence of the group prior. This technique stabilizes predictions and reflects the clinical fact that a patient’s lesion category remains constant across adjacent images.

4. Meta-classifier: A multinomial logistic regression model trained on \mathbf{h} determines the final decision:

$$\hat{y} = \arg \max_c \sigma(\mathbf{W}\mathbf{h} + \mathbf{b})_c, \quad (3)$$

where σ denotes the softmax function.

IHML produces substantially more stable and reliable predictions than any individual classifier because it combines diverse learners, leverages the uncertainty structure, and enforces patient-level consistency. Unlike end-to-end tabular architectures that directly optimize class scores, IHML decouples evidence extraction from decision fusion, enabling stable aggregation of heterogeneous signals and explicit modeling of predictive uncertainty. This design reduces sensitivity to feature redundancy, stabilizes predictions under class imbalance, and improves robustness when training data is limited. Unlike conventional stacking ensembles that directly learn from raw

feature concatenations, IHML operates entirely in probability space, explicitly modeling predictive uncertainty and intra-patient correlation. The incremental posterior refinement step can be interpreted as a group-consistent Bayesian smoothing process, which is absent in standard ensemble or deep tabular architectures.

4. EXPERIMENTS AND RESULTS

4.1. Experimental Setup

To conduct a thorough, unbiased examination, we separated our dataset by patient. To create an “unseen” test set, we isolated 15% of patients. This data was used solely for the final evaluation, never for training or tuning. Data from 85% of patients were used to construct the models. Five-fold StratifiedGroupKFold cross-validation was performed on the development set. This prevents data from a single patient from appearing in both the training and validation folds, thereby enhancing model generalizability to new subjects. All models were trained and tested using the same patient split, with performance reported on the 15% unseen patient test set.

4.2. Performance Comparison on Models

We evaluated a wide range of models on the fused multimodal feature representation, including both classical machine-learning approaches and modern deep tabular learning methods. The conventional baselines include logistic regression,

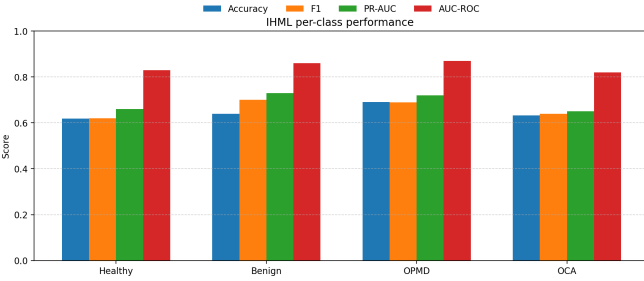


Fig. 3. Per-class performance of the proposed IHML model on the held-out patient-wise test set.

random forest, support vector machines (SVM), XGBoost, and LightGBM, which capture a variety of linear and non-linear decision boundaries and serve as base learners in the proposed IHML architecture. In addition, we tested several new deep tabular architectures, including TabICL [12], T2G-Former [13], TabTransformer [14], and DANet [15], which have recently demonstrated excellent performance on heterogeneous tabular data.

Table 1 presents the comparison results. While numerous deep tabular models perform well, the proposed Incremental Heuristic Meta-Learner (IHML) consistently beats both traditional machine-learning baselines and current deep tabular approaches on all evaluation measures. This demonstrates the efficiency of combining heterogeneous calibrated learners, uncertainty-aware probabilistic features, and patient-level posterior smoothing to achieve robust oral lesion classification. Figure 3 shows that the proposed methodology balances classification metrics across healthy, benign, OPMD, and OCA categories, minimizing class imbalance while preserving minority-class performance.

Table 1. Comparison results with classical machine-learning models and deep tabular approaches on the patient-wise held-out test set. Underlined numbers represent second-best outcomes, whereas bold values represent best results.

Model	Macro F1	Accuracy	PR-AUC	AUC-ROC
Logistic Regression	44.03	47.10	45.86	71.70
Random Forest	<u>58.08</u>	<u>58.82</u>	<u>65.24</u>	<u>81.03</u>
SVM	54.20	54.41	63.45	81.47
XGBoost	55.44	57.35	66.65	82.54
LightGBM	<u>61.27</u>	59.81	<u>67.51</u>	82.89
TabICL	57.14	60.29	62.04	78.99
T2G-Former	<u>44.51</u>	49.35	48.57	74.98
TabTransformer	47.21	47.79	50.38	71.42
DANet	57.20	<u>61.76</u>	66.03	83.09
IHML	66.23	64.56	69.10	84.45

4.3. Ablation Study

We conducted a stepwise ablation study, incrementally adding feature groups to the baseline and measuring the contribution

of each feature family within the IHML framework. Table 2 reports five configurations (M1-M5), with checkmarks indicating the presence of a feature block and crosses representing its removal. Model M1 only embeds ConvNeXt. M2 includes demographic characteristics indicating patient clinical priors. M3 uses haemoglobin-sensitive descriptors from the reconstructed spectral cube. M4 adds texture information, while M5 has all spectrum descriptors. The steady improvement proves that each feature family provides supplementary information. Ablation analysis proves multimodal fusion works.

Table 2. Ablation study evaluating the contribution of individual feature groups within the IHML framework. **D** denotes demographic features, **H** denotes haemoglobin-sensitive spectral biomarkers, **T** denotes multiscale texture and structural descriptors, and **S** denotes spectral-shape and unmixing-oriented features.

Model	D	H	T	S	Macro F1	Acc.	PR-AUC	AUC-ROC
M1	✗	✗	✗	✗	54.97	52.52	64.44	83.86
M2	✓	✗	✗	✗	60.08	58.27	68.12	81.03
M3	✓	✓	✗	✗	63.19	62.24	63.38	82.84
M4	✓	✓	✓	✗	64.13	62.55	67.07	82.27
M5	✓	✓	✓	✓	66.23	64.56	69.10	84.45

5. CONCLUSION

We presented a multimodal fusion framework for oral lesion classification that integrates deep visual embeddings, spectrally enriched descriptors, and clinical priors. Our method uses deep morphological embeddings, haemoglobin-sensitive spectral indications, texture descriptors, and demographic data. Each modality captures lesion appearance and clinical context uniquely. RGB pictures were converted to 31-band hyperspectral images. These extracted spectral-style biomarkers are not available in RGB imaging. We created tiny texture and spectral-shape characteristics to capture local structure and wavelength-dependent variations. We proposed integrating various features into IHML. IHML combines calibrated base learners, uncertainty-aware meta-features, and patient-level smoothing. This strategy improves stability and consistency in patient forecasts. Our strategy was tested on an unobserved patient split. IHML has a macro F1-score of 66.23% and an AUC-ROC of 84.45%. Our findings beat all baseline models. Each feature block yielded considerable gains in the ablation research. Our findings demonstrate that incorporating deep, spectral, and clinical information enhances oral lesion categorization. Future work will explore end-to-end multimodal attention architectures with explicit uncertainty modeling, as well as validation on physically acquired hyperspectral datasets.

6. REFERENCES

[1] World Health Organization, “Global oral health status report: towards universal health coverage for oral health by 2030,” 2022.

[2] N.S. Piyarathne, S.N. Liyanage, R.M.S.G.K. Ranayaka, P.V.K.S. Hettiarachchi, G.A.I. Devindi, F.B.A.H. Francis, D.M.D.R. Dissanayake, R.A.N.S. Ranasinghe, M.B.D. Pavithya, I.B. Nawinne, R.G. Ragel, and R.D. Jayasinghe, “A comprehensive dataset of annotated oral cavity images for diagnosis of oral cancer and oral potentially malignant disorders,” *Oral Oncology*, vol. 156, pp. 106946, 2024.

[3] Syed Waqas Zamir, Aditya Arora, Salman Khan, Munawar Hayat, Fahad Shahbaz Khan, Ming-Hsuan Yang, and Ling Shao, “Multi-stage progressive image restoration,” *2021 IEEE/CVF Conference on Computer Vision and Pattern Recognition (CVPR)*, pp. 14816–14826, 2021.

[4] Sanghyun Woo, Shoubhik Debnath, Ronghang Hu, Xinlei Chen, Zhuang Liu, In So Kweon, and Saining Xie, “ConvNeXt V2: Co-designing and scaling convnets with masked autoencoders,” *2023 IEEE/CVF Conference on Computer Vision and Pattern Recognition (CVPR)*, pp. 16133–16142, 2023.

[5] Guolin Ke, Qi Meng, Thomas Finley, Taifeng Wang, Wei Chen, Weidong Ma, Qiwei Ye, and Tie-Yan Liu, “LightGBM: A highly efficient gradient boosting decision tree,” *Advances in Neural Information Processing Systems*, vol. 30, 2017.

[6] Manu Parmar, Steven Lansel, and Brian A. Wandell, “Spatio-spectral reconstruction of the multispectral datacube using sparse recovery,” *2008 15th IEEE International Conference on Image Processing*, pp. 473–476, 2008.

[7] Tarek Stiebel, Simon Koppers, Philipp Seltsam, and Dorit Merhof, “Reconstructing spectral images from RGB-images using a convolutional neural network,” *2018 IEEE/CVF Conference on Computer Vision and Pattern Recognition Workshops (CVPRW)*, pp. 1061–10615, 2018.

[8] Yuzhi Zhao, Lai-Man Po, Qiong Yan, Wei Liu, and Tingyu Lin, “Hierarchical regression network for spectral reconstruction from RGB images,” *Proceedings of the IEEE/CVF Conference on Computer Vision and Pattern Recognition Workshops*, pp. 422–423, 2020.

[9] Yuan Guo, Yixiang Huang, Changping Huang, Xuejian Sun, Qingxian Luan, and Lifu Zhang, “Non-invasive assessment of periodontal inflammation by continuum-removal hemodynamic spectral indices,” *European Journal of Medical Research*, vol. 29, no. 1, pp. 193, 2024.

[10] Buddhadev Goswami, Susmit Neogi, Saurabh Nagar, Nirmal Punjabi, and Ravindra Gudi, “Classification of oral potentially malignant disorders using multimodal feature integration,” *2025 IEEE International Symposium on Biomedical Imaging (ISBI)*, 2025.

[11] Steven L Jacques, “Optical properties of biological tissues: a review,” *Physics in Medicine and Biology*, vol. 58, no. 11, pp. R37–R61, 2013.

[12] Jingang QU, David Holzmüller, Gaël Varoquaux, and Marine Le Morvan, “TabICL: A tabular foundation model for in-context learning on large data,” *Forty-second International Conference on Machine Learning (ICML)*, 2025.

[13] Jiahuan Yan, Jintai Chen, Yixuan Wu, Danny Z Chen, and Jian Wu, “T2g-former: organizing tabular features into relation graphs promotes heterogeneous feature interaction,” *Proceedings of the AAAI Conference on Artificial Intelligence*, vol. 37, no. 9, pp. 10720–10728, 2023.

[14] Xin Huang, Ashish Khetan, Milan Cvitkovic, and Zohar Karnin, “Tabtransformer: Tabular data modeling using contextual embeddings,” *arXiv preprint arXiv:2012.06678*, 2020.

[15] Jintai Chen, Kuanlun Liao, Yao Wan, Danny Z Chen, and Jian Wu, “DAnets: Deep abstract networks for tabular data classification and regression,” *Proceedings of the AAAI Conference on Artificial Intelligence*, vol. 36, no. 4, pp. 3930–3938, 2022.